

Enhancing static and dynamic magnetic properties of Mg-Zn doped Co₂Y-type hexaferrite as broadband microwave absorbing material

M. H. SHAMS, A. S. H. ROZATIAN*, M. H. YOUSEFI

Department of Physics, University of Isfahan, Hezar Jarib Street, Isfahan 81746-73441, Iran

New Ba₂Co_{2-x}(MgZn)_xFe₁₂O₂₂ (x=0, 0.5, 1, 2) Y-type hexaferrites were synthesized by solid state ceramic method to tailor their electromagnetic properties. Subsequently, the effects of Mg²⁺ and Zn²⁺ dopants on the static and dynamic magnetic properties at 300 MHz to 40 GHz were studied. The crystalline structure, particle size and static and dynamic magnetic properties were investigated by X-ray diffraction (XRD), scanning electron microscopy (SEM), vibrating sample magnetometer and vector network analyzer, respectively. The results showed that the saturation magnetization and the complex permeability values have been increased while the coercive field and the resonance frequency decreased by increasing the amount of dopants. The reflection loss and thickness of composite samples were optimized based on the maximum RL bandwidth for -10 dB. Compared with pure Co₂Y-type hexaferrite, Mg-Zn doped Co₂Y-type hexaferrite composites exhibited enhanced absorbing properties at S, C, X and Ku frequency bands.

(Received March 16, 2015; accepted May 7, 2015)

Keywords: Microwave material, Barium hexaferrite, Magnetic properties, Solid state ceramic method

1. Introduction

Wireless communication industry has grown beyond expectations. As such, it has entered everyday life and captured the attention of the media and the imagination of the public. Many new applications, including wireless systems coupled with computers, smart homes, remote telemedicine and wireless sensors involve a lot of electromagnetic wave pollution [1]. Therefore, microwave absorbing materials are required to alleviate these pollutions by absorbing the unwanted microwave. New radars have also been developed and radar absorbing materials are, therefore, necessary to design stealth objects.

The microwave losses are correlated with the particle size, morphology, microstructure and other characteristics of the material [2-5]. An efficient EM wave absorbing material should be capable of enough loss with a sufficient absorption bandwidth. Minimum reflection depends on the impedance matching of the material with the free space. The impedance matching is associated with the relative complex permeability ($\mu_r = \mu'_r - j\mu''_r$), relative complex permittivity ($\epsilon_r = \epsilon'_r - j\epsilon''_r$) and thickness. When the impedance is matched completely with two media, the wave is entered without any reflection from the interface. The entered wave can lose its energy through dielectric and magnetic loss mechanisms and it is converted into heat. An absorbing material should be able to cause favorable loss in the necessary frequency range. In order to achieve maximum loss in a vast frequency range, selecting the material and controlling its dielectric and magnetic properties are of high importance. So far, various materials have been studied to evaluate their capability in absorbing EM waves. Among these materials, the ferrites are widely used due to their absorbing power. Depending on their

crystalline and chemical composition, ferrites perform differently in different frequency ranges. Spinel ferrites are mostly utilized in a range from few MHz to GHz [6-9] such that their absorbing power may be reduced due to Snoek's limit [10]. Hexaferrites, are capable of absorbing higher power in GHz frequencies [11,12]. Hexaferrites, depending on their chemical compositions, are divided into M, W, Y, U, X and Z-types [13].

Among the hexaferrites, the Y-type hexaferrite (Ba₂Me₂Fe₁₂O₂₂) is constructed from the basic units of hexagonal barium M-type and cubic spinel ferrites which retain a hexagonal structure, usually with the direction of magnetization being parallel to the c-axis [11,14]. It has a good potential to control magnetic and electrical properties for better tuning in microwave range by substituting Ba, Fe, and Me with divalent and trivalent ions [15-17]. Often, by substituting Fe and/or Me with a large amount of other ions, the magnetocrystalline anisotropy can be greatly reduced, and even switched from a c-axis to the basal plane. This can reduce the saturation magnetization and hence, permeability. The characteristic of magnetocrystalline planar anisotropy and high initial permeability made the Y-type hexaferrite attractive for microwave absorbing [18].

Moreover, most studies of Y-type hexaferrite have been focused on magnetic and dielectric properties with a view to explore magneto-electric and microwave device applications (for example, see Refs. [19] and [20]). However, there have been few studies regarding the complex permittivity, permeability and microwave absorbing properties of Y-type hexaferrite at GHz range.

In the present work, new doped Co₂Y-type hexaferrites, Ba₂Co_{2-x}(MgZn)_xFe₁₂O₂₂ (x=0, 0.5, 1, 2), were synthesized by the conventional solid state method.

We investigated the effect of the concentration of dopants on the microstructure, magnetic properties, complex permittivity, complex permeability and microwave absorbing characteristics in the range of 300 MHz to 40 GHz.

2. Experiments

Analytical grade chemicals such as barium carbonate (BaCO₃), iron oxide (Fe₂O₃), cobalt oxide (Co₃O₄), magnesium oxide (MgO) and zinc oxide (ZnO) were used to synthesize the stoichiometric compositions as the starting materials. In order to obtain the composition of Ba₂Co_{2-x}(MgZn)_xFe₁₂O₂₂ (x=0, 0.5, 1, 2), the Co²⁺ ions were replaced by Mg²⁺ and Zn²⁺ dopants (with equal ratio). The starting materials were mixed in a planetary mill for 1 hour and sintered in air at 1150 °C for 3 hours. The heating rate was 6 °C/min up to 600 °C and then the rate was decreased to 3 °C/min to reach 1150 °C and kept at the sintering temperature for 3 hours. Finally, the sintered ferrite was crushed in a planetary mill for 1 hour to obtain the fine powders. The samples were prepared with 70 wt% of the powder and 30 wt% of paraffin. The powder was mixed with paraffin dissolved to homogenize toluene. Then, it was heated at 80 °C for 10 h to remove the toluene. The as-prepared composite samples were made in the form of the standard rings (outer diameter: 7 mm, inner diameter: 3.04 mm, thickness: 2 mm) and rectangles (with two various sizes – length: 10.66 mm, width: 4.31 mm, thickness: 2 mm and length: 7.11 mm, width: 3.55 mm, thickness: 1.5 mm).

The composition and the crystalline phases were identified by an X'Pert Pro MPD PANalytical diffractometer using Cu K α radiation ($\lambda=1.5406$) with a scanning rate of 0.0260 degrees at room temperature. The characteristic lattice parameters, a and c , were calculated according to the following formula [21]:

$$\frac{1}{d_{hkl}^2} = \frac{4(h^2+hk+k^2)}{3a^2} + \frac{l^2}{c^2} \quad (1)$$

where h , k and l are Miller indices and d is interplanar spacing as determined by the Bragg formula, $2d\sin\theta = n\lambda$. The unit cell volume was calculated from the lattice parameters a and c using the following formula [22]:

$$V_{cell} = \frac{\sqrt{3}}{2} a^2 c \quad (2)$$

The X-ray density, ρ_x of the material was calculated according to the relation:

$$\rho_x = \frac{2M}{N_a V_{cell}} \quad (3)$$

where M represents the molar mass of the sample, and N_a is Avogadro's number.

Electron micrographs were taken using a LEO 435VP Scanning Electron Microscopy (SEM). The

particle size of the samples was estimated from SEM imaging. The magnetization measurements were carried out using VSM measurement. The coercive field and magnetic remanence were obtained directly from the M-H loop and the saturation magnetization was calculated from the law of approach to saturation [23].

The electromagnetic S-parameters of composite samples prepared with transmission/reflection method were measured using standard 7 mm coaxial airline, WR42 and WR28 rectangular waveguides fixtures through a ZVK vector network analyzer in the range of 300 MHz to 40 GHz. The complex permittivity and permeability were extracted from the measured electromagnetic S-parameters by utilizing the Nicolson–Ross–Weir algorithm [24].

The reflection loss (RL) of a microwave absorbing layer with metal back was calculated based on the values of relative complex permeability and permittivity values in terms of frequency and thickness of the layer by the following formulas [25]:

$$RL = 20 \log \left(\frac{jZ \tanh(kd) - 1}{jZ \tanh(kd) + 1} \right) \quad (4)$$

$$Z = \sqrt{\frac{\mu_r}{\epsilon_r}} \quad (5)$$

$$k = \frac{2\pi f}{c} \sqrt{\mu_r \epsilon_r} \quad (6)$$

where Z is the impedance of the absorber medium, μ_r and ϵ_r are relative complex permeability and permittivity, d is the thickness of the absorbing layer, c is the velocity of light, and f is the wave frequency.

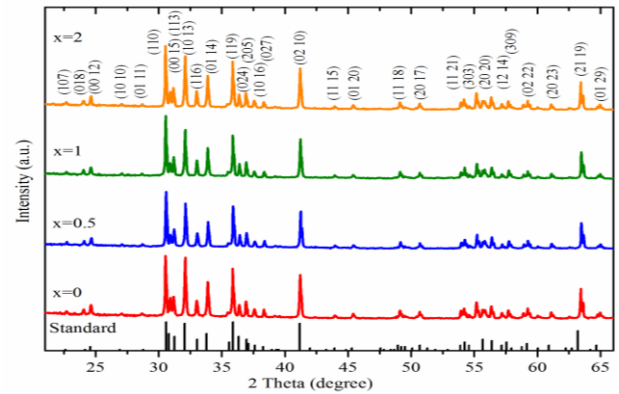


Fig. 1. X-ray diffraction patterns of doped barium ferrites Ba₂Co_{2-x}(MgZn)_xFe₁₂O₂₂ (x=0, 0.5, 1, 2) powders.

3. Results and discussion

Fig. 1 shows the XRD pattern of the samples. The peaks for the doped Co₂Y-type hexaferrites appeared at the same positions as those of the undoped ones, but with different intensities. The patterns revealed that single phase materials were formed that were similar to the standard XRD pattern of Co₂Y-type hexaferrite

($\text{Ba}_2\text{Co}_2\text{Fe}_{12}\text{O}_{22}$). The crystal structure was determined to be a single-phased rhombohedral with the space group being R-3m. The lattice parameters "a" and "c" for the pure Co_2Y -type hexaferrite, $\text{Ba}_2\text{Co}_{2-x}(\text{MgZn})_x\text{Fe}_{12}\text{O}_{22}$ ($x=0, 0.5, 1, 2$), are determined and listed in Table 1, as shown in Fig. 2(a). The values of the pure one were different and near the value of the standard JCPDS 019-0100 ($a=5.8530$ and $c=43.5090$).

It is known that there is a correlation between the ionic radius and its site occupancy with lattice parameters. As shown in Table 2, the total average radii of Mg^{2+} and Zn^{2+} for octahedral sites were lower than the ionic radius of Co^{2+} , whereas the tetrahedral sites were close to it. Thus, with raising the doping concentration, the contraction in the lattice parameters was expected, but we observed anomalous behavior in the variation of the lattice parameters as shown in Fig. 2(a). This anomaly could originate from the different preference in site occupation of Mg^{2+} and Zn^{2+} when it substituted Co^{2+} [26].

The metallic cations (Me) and iron ions could be distributed to six crystallographic sites: two tetrahedral sites ($6c_{IV}$ and $6c_{IV}^*$) and four octahedral sites ($3a_{VI}$, $18h_{VI}$, $6c_{VI}$ and $3b_{VI}$) as indicated in Table 3 [27,28]. It has been previously reported that Co^{2+} ions prefer to occupy octahedral sites ($6c_{VI}$, $18h_{VI}$, $3b_{VI}$ and $3a_{VI}$) [27], Zn^{2+} ions tend to occupy tetrahedral sites ($6c_{IV}$ and $6c_{IV}^*$) [28,29] and Mg^{2+} tend to occupy octahedral sites ($6c_{VI}$ and $3b_{VI}$) [27,30]. The parameter 'a' was contracted for $x=0.5$ and expanded by raising doping concentration as depicted in Fig. 2(a). When Co^{2+} ions substituted with the Mg-Zn ions, Zn^{2+} ions preferred occupation of tetrahedral sites. Accordingly, Fe^{3+} ions in tetrahedral sites would migrate to the octahedral site. Occupation of Fe^{3+} and Mg^{2+} ions at the octahedral sites in place of the larger Co^{2+} ions led to the contraction of the 'a' parameter. On the contrary, by raising the doping concentration, the lattice distortion was increased, leading to the expansion of 'a' parameter.

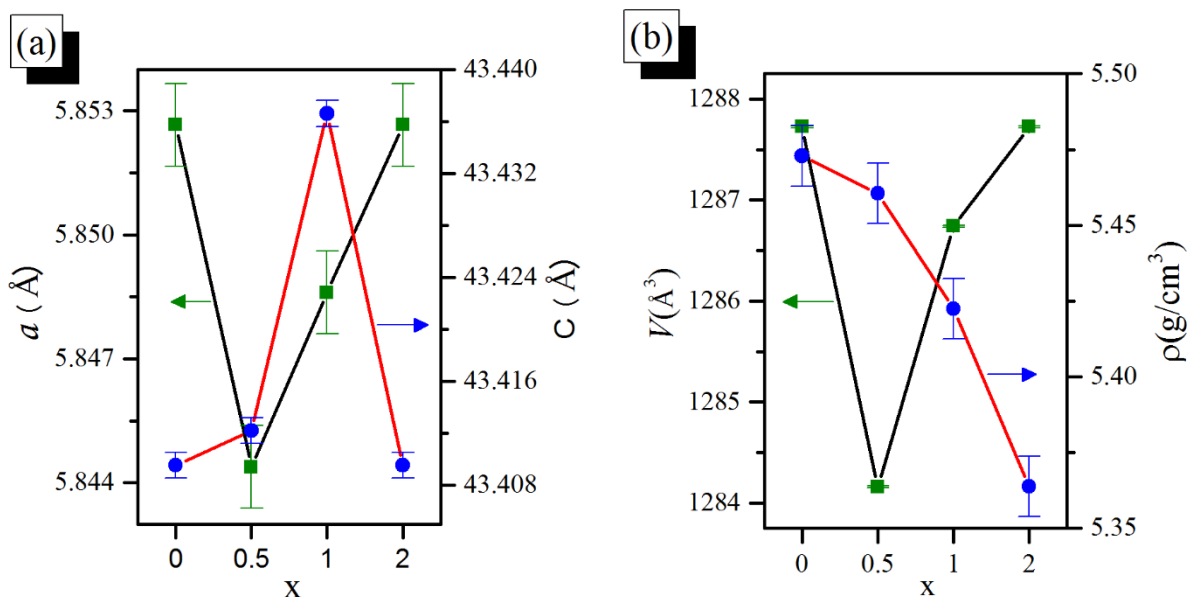


Fig. 2. a) The a (rectangle in green) and c (circle in blue) lattice parameters vs. the amount of Mg-Zn dopants and b) the X-ray unit cell volume (rectangle in green) and X-ray density (circle in blue) vs. the amount of Mg-Zn dopants.

Table 1. Lattice parameters a and c, c/a ratio, X-ray unit cell volume and X-ray density vs. the amount of Mg-Zn dopants.

x	a (Å)	c (Å)	c/a	V (Å ³)	ρ (g/cm ³)
JCPDS	5.853	43.509	7.433	1290.82	5.35
0	5.852	43.409	7.417	1287.72	5.47
0.5	5.844	43.412	7.428	1284.16	5.46
1	5.848	43.436	7.426	1286.73	5.42
2	5.852	43.409	7.417	1287.72	5.36

Table 2. Electronic configuration and ionic radii of various cations in octahedral and tetrahedral coordination [31].

Metallic Ion	Elect. Confi.	Ionic Radius (\AA)	
		Octah.	Tetra.
Fe^{3+a}	$3d^5$	0.645	0.49
Co^{2+a}	$3d^7$	0.745	0.58
Mg^{2+}	$2p^6$	0.72	0.57
Zn^{2+}	$3d^{10}$	0.74	0.6
Mg-Zn^b	---	0.73	0.585

^aOn the assumption of high spin radius.

^bAverage of ionic radii in each coordination.

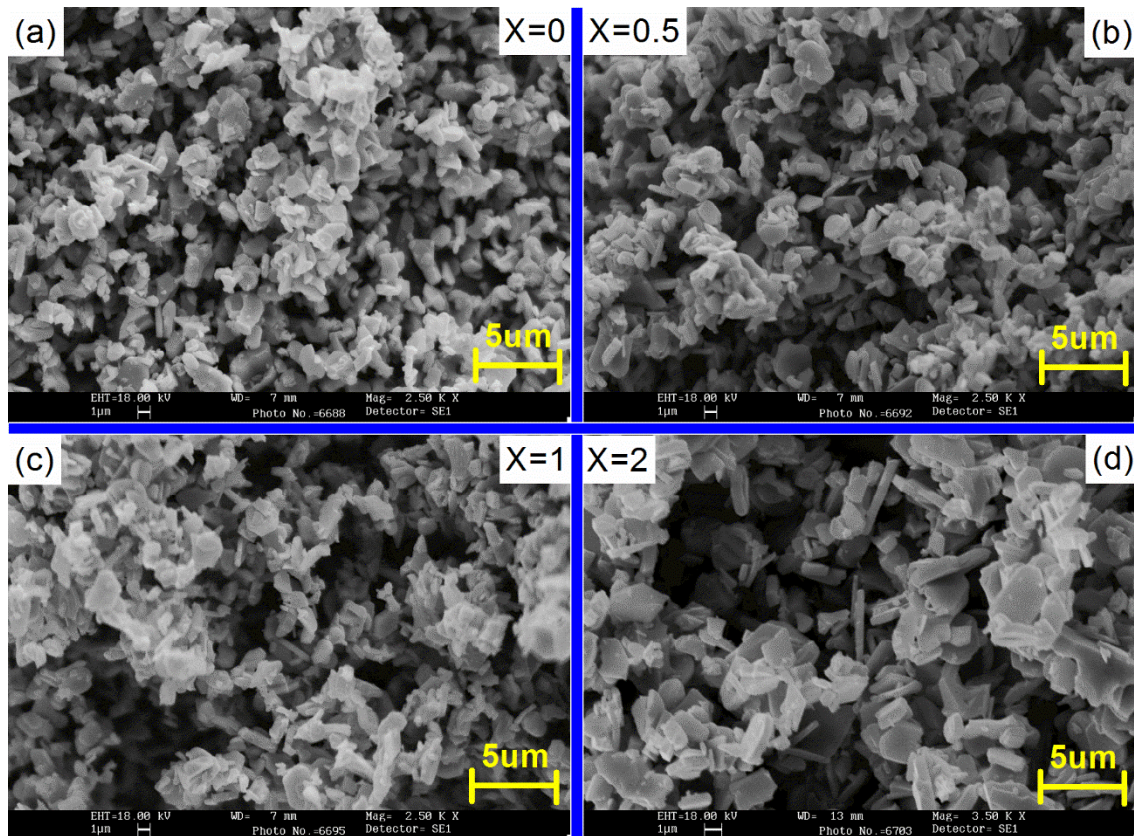


Fig. 3. The distribution of particles for the un-doped and doped Co_2Y -type barium hexaferrites a) $x=0$, b) $x=0.5$, c) $x=1$ and d) $x=2$. The particles had a hexagonal plate shape with the size of about 2 to 5 μm .

Table 3. Various metallic sub-lattices, coordination, block, the number of ions and spin orientation for the Y-type ferrite structure.

Sub-lattice	Coordination	Block	Number of ions per unit cell	Spin
$6c_{IV}$	Tetrahedral	S	6	down
$3a_{VI}$	Octahedral	S	3	up
$18h_{VI}$	Octahedral	S-T	18	up
$6c_{VI}$	Octahedral	T	6	down
$6c_{IV}^*$	Tetrahedral	T	6	down
$3b_{VI}$	Octahedral	T	3	up

The parameter 'c' was expanded from $x=0$ to $x=1$ and contracted for $x=2$ as depicted in Fig. 2(a). It can be explained by the weakening of the super-exchange interaction caused by replacing magnetic ions with the nonmagnetic ions [28]. The strongest super-exchange

interaction was the $3b_{VI}-6c_{IV}^*$; moreover, the only appreciable perturbing interaction was $6c_{VI}-6c_{IV}^*$, both belonging to the T block. The entrance of a nonmagnetic ion in $3b_{VI}$ sites might cause a drastic change in the magnetic order. The upper and lower parts of the unit cell

were linked by the strong interaction of these sites with six ions $6c_{IV}^*$. Also, the partial substitution of iron ions in $6c_{VI}$ sites resulted in breaking the inversion symmetry around $3b_{VI}$ sites. Accordingly, anti-symmetric interactions $6c_{VI}$ - $3b_{VI}$ and $18h_{VI}$ - $3b_{VI}$ could be appreciable and the anti-symmetric exchange vector had to be parallel to the c-axis [27] and the contraction in 'c' parameter for $x=2$ was

observed. The distribution of particles for the un-doped and doped Co_2Y -type barium hexaferrites ($x=0, 0.5, 1$ and 2) are shown through the SEM images in Fig. 3. The images indicated that the particles had a hexagonal plate shape with the size of about 2 to $5 \mu m$.

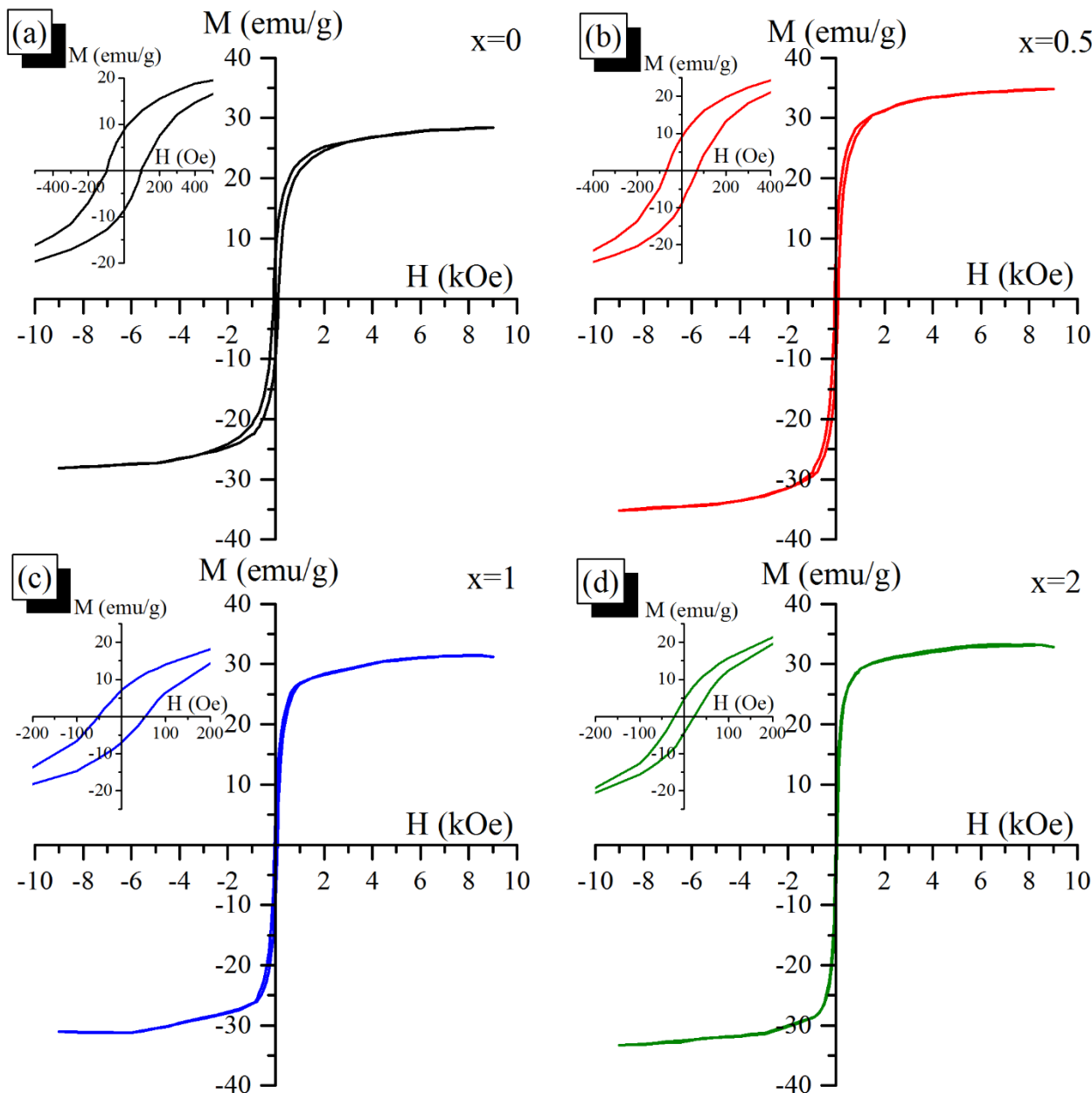


Fig. 4. Hysteresis loops measured at room temperature of $Ba_2Co_{2-x}(MgZn)_xFe_{12}O_{22}$ ($x=0, 0.5, 1, 2$) samples.

Fig. 4 shows the magnetic hysteresis loops of the samples at room temperature. The M-H loops indicated that all samples had a ferrimagnetic behavior. The Mg-Zn content dependence of the M_s and H_c is shown in Fig. 5 and listed in Table 4. The M_s of the undoped sample ($x=0$) was 29 emu/g , consistent with the reported values [16,32]. As shown in, Fig. 5 the anomalous behavior in the

variation of the M_s with raising the amount of dopants was clearly observed. This could be due to the different preference in the site occupation of Mg^{2+} and Zn^{2+} when they substituted Co^{2+} . Also, this was found to be in agreement with the results of lattice parameters shown in Fig. 2 (a). As mentioned before, Zn^{2+} ions prefer occupation of tetrahedral sites $6c_{IV}$ (spin down) and $6c_{IV}^*$

(spin down) while Mg²⁺ tend to occupy octahedral sites 6c_{VI} (spin down) and 3b_{VI} (spin up). When the magnetic ions in the spin down sites were replaced by the non-magnetic ions, we expected an increase in the net magnetization. Also, substitution of the spin up sites caused the net magnetization decrease. Therefore, the reduction of M_s for x=1 and x=2 could be due to the occupation of 3b_{VI} sites by Mg²⁺ ions. This was consistent with the reported values for Zn₂Y-type [32-34] and Mg₂Y-type [27,35] hexaferrites.

Values of the magnetic remanence (M_r) versus x are also listed in Table 4. By raising the amount of dopants from x=0 to x=0.5, M_r remained constant while it was decreased by the further amount of dopants. M_r is a strong function of the chemical composition, density and orientation. Therefore, it was expected that the decrease in the density of the ferrite or the substitution of the nonmagnetic ions would result in the reduction of M_r. Fig. 2(b) shows a linear decrease in the unit cell X-ray density with an increase in the substitution level which is compatible with result in Table 4.

Nevertheless, there was no change in M_r when x was varied from 0 to 0.5. This observation could be associated to the increase in the magnetization for x = 0.5. As the density was decreased, the magnetization increased. Therefore, there was probably a counterbalance between these opposite variations and consequently, M_r remained constant. Similar discussion have been reported by Jazirehpour et al. [36] for BaFe_{12-x}(MgTi)_xO₁₉ (x=0, 1, 2) samples. In the rest of the x range, both magnetization in average and density had a decreasing trend, thus a making it inevitable for M_r.

Table 4. Magnetic properties of Ba₂Co_{2-x}(MgZn)_xFe₁₂O₂₂ (x=0, 0.5, 1, 2) powders at room temperature.

x	M _s (emu/g)	M _r (emu/g)	H _c (Oe)	f _{FMR} (GHz)	μ'' (FMR)
0	29	8.7	98	6.4	0.32
0.5	35.5	9	70	5.7	0.48
1	32	7.1	54	4.7	0.78
2	34	4.6	23	3.1	0.96

The behaviour of the coercivity was consistent with the general behaviour of the anisotropy field and saturation magnetization [37]. It is known that when a non-magnetic ion occupies the octahedral site, the magnetic anisotropy is reduced through either dilution of the off-centred Fe³⁺ sites or the reduction of their off-centering deformation [38]. Here, the occupation of Mg²⁺ in the octahedral Fe³⁺ sites seemed to reduce the magnetic anisotropy. Moreover, it has been reported that the anisotropy field decreases with Zn²⁺ doping [26,28,33] although Zn²⁺ prefers to occupy the tetrahedral sites as mentioned before. Therefore, the reduction in the coercivity with the increasing amount of dopants(x) could be associated with the decrease in the anisotropy field.

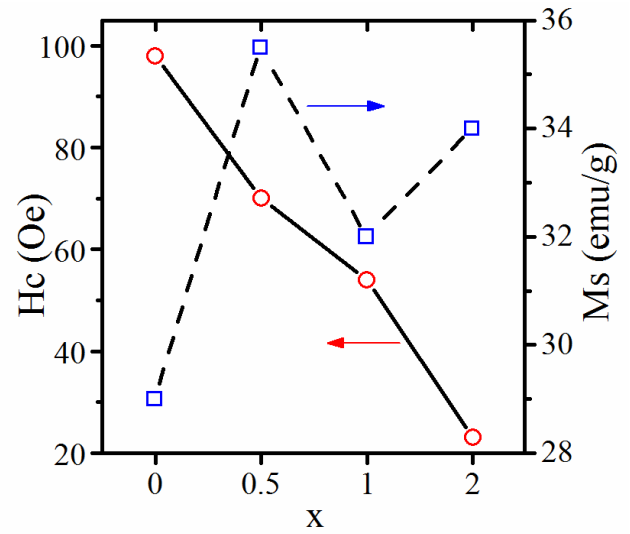


Fig. 5. Variation of saturation magnetization, M_s, and coercivity, H_c, versus the amount of Mg-Zn dopants (x).

The complex μ_r and ε_r spectra of composite samples are shown in Fig. 6, from 300 MHz to 40 GHz. The μ_r' and μ_r'' values were increased by raising the amount of dopants while ε_r' and ε_r'' demonstrated a slight change and weak frequency dependence within the frequency range. The conduction mechanism in ferrite could be attributed to the easy electron transfer between Fe²⁺ and Fe³⁺ as it had some effect on the permittivity. The observed decrease in magnetic permeability could be due to the reduction of M_s and Eddy current loss [39]. For the application in microwave absorption, the initial permeability (μ_i) of an absorber should be as high as possible, and the permeability of ferromagnetic materials can be expressed as [40]:

$$\mu_i = \frac{M_s^2}{(akH_cM_s + b\lambda\xi)} \quad (7)$$

where a and b are two constants determined by the material composition, λ is the magnetostriction constant, and ξ is an elastic strain parameter of the crystal. It can be seen from equation (4) that both higher M_s and lower H_c are favorable to the improvement of the μ_i value, which in turn would enhance the microwave absorption. It is clearly observed in Fig. 5, that the M_s is increased and the H_c decreased with raising the amount of dopants(x) for Ba₂Co_{2-x}(MgZn)_xFe₁₂O₂₂. It can be clearly seen in Fig. 3 that particles had a hexagonal plate-shape. Therefore, the ferromagnetic resonance frequencies are reduced due to the demagnetizing contribution of plate-shape particles [41].

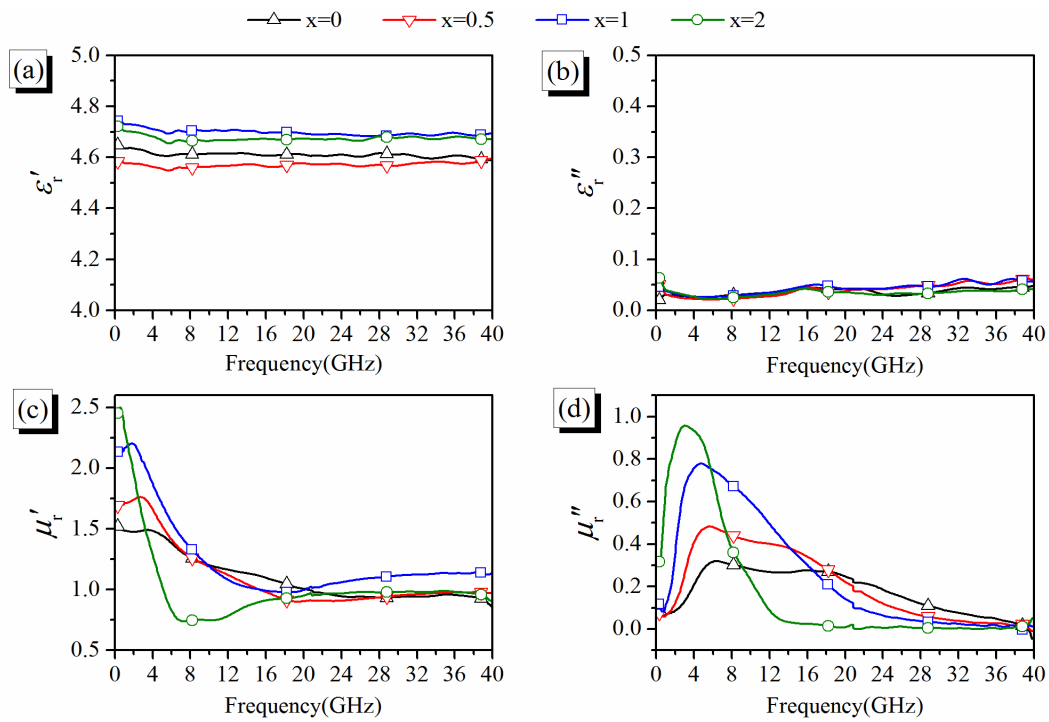


Fig. 6. The relative complex permittivity and permeability measured at room temperature of $Ba_2Co_{2-x}(MgZn)_xFe_{12}O_{22}$ ($x=0, 0.5, 1, 2$) composite samples.

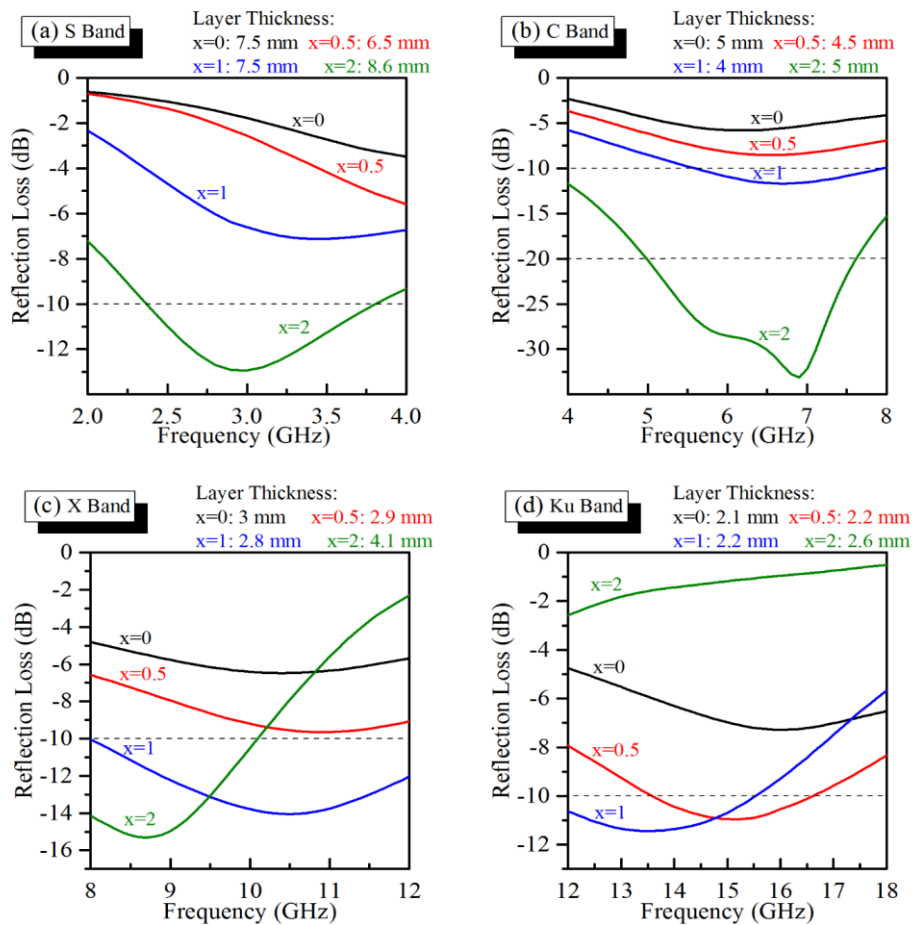


Fig. 7. Optimal reflection loss plots of $Ba_2Co_{2-x}(MgZn)_xFe_{12}O_{22}$ ($x=0, 0.5, 1, 2$) composite samples in different frequency bands: (a) S band, (b) C band, (c) X band and (d) Ku band.

This reduction in FMR was clearly seen in Fig. 6(d). The peak of resonance frequencies in μ_r'' spectra appeared about 2 to 5 GHz with a broad band behavior, which was in agreement with previously reported works [41-43]. The relevant data for f_{FMR} and $\mu_r''(\text{FMR})$ are listed in Table 4. The value of μ_r'' at ferromagnetic resonance was increased with amount of Mg-Zn.

The optimal reflection loss plots of Ba₂Co_{2-x}(MgZn)_xFe₁₂O₂₂ (x=0, 0.5, 1, 2) composite samples in different frequency bands are shown in Fig. 7. These plots were calculated with a computer code which found the optimal thickness for each material by receiving ϵ_r and μ_r complex coefficients in different frequency bands based on the maximum RL bandwidth for -10 dB. The sample x=2 had some RL value below -10 dB at 72 and 100 percent of S and C bands, respectively. Moreover, the composite sample with x=2 showed a good performance by absorbing intensity below -20 dB at 67 percent of the C band. Also, the sample x=1 had some RL value below -10 dB at 100 and 58 percent of X and Ku bands, respectively. It was found that samples with x=1 and 2 performed better than the other two samples in terms of microwave absorption.

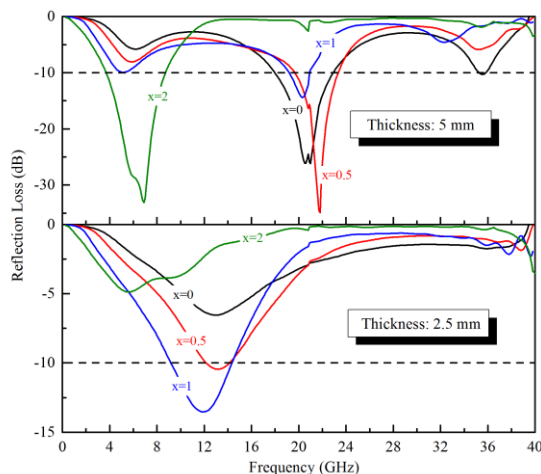


Fig. 8. Reflection loss plots of Ba₂Co_{2-x}(MgZn)_xFe₁₂O₂₂ (x=0, 0.5, 1, 2) composite samples in two different thicknesses, 2.5 mm and 5 mm, vs. frequency.

Fig. 8 shows the frequency dependence of reflection loss of the composite samples with the thickness of 2.5 and 5 mm. It was clearly observed that Ba₂Co_{2-x}(MgZn)_xFe₁₂O₂₂ (x=0, 0.5, 1, 2) composite materials could be applied as a wide bandwidth radar absorbing or EMI material at different frequency bands.

The analysis of a metal-backed ferrite layer revealed two matching conditions [44]. The first matching condition was due to the material properties, where the relative permittivity and relative permeability were equal to each other, while the second matching condition was due to the cancellation of the incidence and the reflected waves in the absorber layer when the thickness was equal to $n\lambda/4$, where n is an odd integer and λ is the wavelength

in the materials. It can be clearly observed in Fig. 6 that the values of permittivity and permeability were not equal. Accordingly, the first matching condition could not occur and all dips were related to matching thickness.

4. Conclusion

Single phase Co₂Y-type hexaferrites Ba₂Co_{2-x}(MgZn)_xFe₁₂O₂₂ (x=0, 0.5, 1, 2) were synthesized with the particle size of about 2-5 μm by the conventional solid state method. Magnetic properties of Co₂Y-type hexaferrites doped with non-magnetic Mg-Zn dopants were characterized, and variation trends of magnetic parameters were studied. Variations of lattice parameters versus the substitution level, in addition to variation trends of magnetic parameters, were used to justify site occupancies of substituent elements and explain the magnetic properties. An anomalous behavior in the variation of the M_s and lattice parameters was observed with raising the amount of dopants, due to the different preference in the site occupation of Mg²⁺ and Zn²⁺ when they substituted Co²⁺. Also, the results showed that the saturation magnetization increased dramatically. The μ' and μ'' values were found to increase by increasing the amount of dopants while ϵ' and ϵ'' demonstrated a slight change and weak frequency dependence within the frequency range. The optimal reflection loss plots of composite samples in different frequency bands were calculated and the optimal thickness for each material was calculated based on the maximum RL bandwidth for -10 dB. Compared with pure Co₂Y-type hexaferrite, Mg-Zn doped Co₂Y-type hexaferrite composites exhibited enhanced absorbing properties with good absorbing performance at S, C, X and Ku frequency bands.

Acknowledgements

The authors would like to thank the Office of Graduate Studies of the University of Isfahan for their support.

References

- [1] Y. Liu, Z. Zhang, S. Xiao, C. Qiang, L. Tian, J. Xu, Applied Surface Science **257**, 7678 (2011).
- [2] Z. Li, G. Lin, L. Chen, Y. Wu, C. Ong, Journal of applied physics **98**, 094310 (2005).
- [3] Z. Zi, J. Dai, Q. Liu, H. Liu, X. Zhu, Y. Sun, Journal of Applied Physics **109**, 07E536 (2011).
- [4] C.-J. Li, B. Wang, J.-N. Wang, Journal of Magnetism and Magnetic Materials **324**, 1305 (2012).
- [5] M. Mehdipour, H. Shokrollahi, Journal of Applied Physics **114**, 043906 (2013).
- [6] K. Khan, S. Rehman, Materials Research Bulletin **50**, 454 (2014).

- [7] M. F. Din, I. Ahmad, M. Ahmad, M. Farid, M. Asif Iqbal, G. Murtaza, M. N. Akhtar, I. Shakir, M. F. Warsi, M. A. Khan, *Journal of Alloys and Compounds* **584**, 646 (2014).
- [8] R. Dosoudil, M. Usakova, A. Grusková, J. Sláma, *Magnetics, IEEE Transactions on* **50**, 1 (2014).
- [9] B. Li, Y. Shen, Z. Yue, C. Nan, *Journal of magnetism and magnetic materials* **313**, 322 (2007).
- [10] J. Snoek, *Physica* **14**, 207 (1948).
- [11] R. C. Pullar, *Progress in Materials Science* **57**, 1191 (2012).
- [12] M. H. Shams, S. M. A. Salehi, A. Ghasemi, *Materials Letters* **62**, 1731 (2008).
- [13] Ü. Özgür, Y. Alivov, H. Morkoç, *Journal of Materials Science: Materials in Electronics* **20**, 789 (2009).
- [14] I. Ali, M. Ahmad, M. Islam, M. Awan, *Journal of sol-gel science and technology* **68**, 141 (2013).
- [15] I. Ali, A. Shakoor, M. Islam, M. Saeed, M. N. Ashiq, M. Awan, *Current Applied Physics* **13**, 1090 (2013).
- [16] M. H. Won, C. S. Kim, *Journal of Applied Physics* **113**, 17D906 (2013).
- [17] G. Murtaza, R. Ahmad, T. Hussain, R. Ayub, I. Ali, M. A. Khan, M. N. Akhtar, *Journal of Alloys and Compounds* **602**, 122 (2014).
- [18] M. Ahmad, I. Ali, M. Islam, M. Rana, *Journal of materials engineering and performance* **22**, 3909 (2013).
- [19] I. Ali, N. Shaheen, M. Islam, M. Irfan, M. N. Ashiq, M. A. Iqbal, A. Iftikhar, *Journal of Alloys and Compounds* **617**, 863 (2014).
- [20] J. Jalli, Y.-K. Hong, J.-J. Lee, G. S. Abo, T. Mewes, B.-C. Choi, S.-G. Kim, *Magnetics Letters, IEEE* **2**, 5000104 (2011).
- [21] M. J. Iqbal, R. A. Khan, S. Takeda, S. Mizukami, T. Miyazaki, *Journal of Alloys and Compounds* **509**, 7618 (2011).
- [22] W. Li, X. Qiao, M. Li, T. Liu, H. Peng, *Materials Research Bulletin* **48**, 4449 (2013).
- [23] R. Grössinger, *physica status solidi (a)* **66**, 665 (1981).
- [24] A. Nicolson, G. Ross, *IEEE Transactions on Instrumentation and Measurement* **19**, 377 (1970).
- [25] Z. Han, D. Li, M. Tong, X. Wei, R. Skomski, W. Liu, Z. Zhang, D. J. Sellmyer, *Journal of Applied Physics* **107**, 09A929 (2010).
- [26] S. Ishiwata, Y. Taguchi, Y. Tokunaga, H. Murakawa, Y. Onose, Y. Tokura, *Physical Review B* **79**, 180408 (2009).
- [27] G. Albanese, M. Carbucchio, A. Deriu, G. Asti, S. Rinaldi, *Applied physics* **7**, 227 (1975).
- [28] S. Mahmood, F. Jaradat, A.-F. Lehlooh, A. Hammoudeh, *Ceramics International* **40**, 5231 (2014).
- [29] S. Lee, S. Kwon, *Journal of magnetism and magnetic materials* **153**, 279 (1996).
- [30] K. Taniguchi, N. Abe, S. Ohtani, H. Umetsu, T.-H. Arima, *Applied physics express* **1**, 031301 (2008).
- [31] R. T. Shannon, *Acta Crystallographica Section A: Crystal Physics, Diffraction, Theoretical and General Crystallography* **32**, 751 (1976).
- [32] C. M. Kim, C. H. Rhee, C. S. Kim, *Magnetics, IEEE Transactions on* **48**, 3414 (2012).
- [33] J. T. Lim, C. S. Kim, *Journal of Applied Physics* **115**, 17A516 (2014).
- [34] S. Bierlich, J. Töpfer, *Journal of Magnetism and Magnetic Materials* **324**, 1804 (2012).
- [35] H. Khanduri, M. C. Dimri, H. Kooskora, I. Heinmaa, G. Viola, H. Ning, M. Reece, J. Krustok, R. Stern, *Journal of Applied Physics* **112**, 073903 (2012).
- [36] M. Jazirehpour, M. Shams, O. Khani, *Journal of Alloys and Compounds* **545**, 32 (2012).
- [37] A. Alsmadi, I. Bsoul, S. Mahmood, G. Alnawashi, K. Prokeš, K. Siemensmeyer, B. Klemke, H. Nakotte, *Journal of Applied Physics* **114**, 243910 (2013).
- [38] S. H. Chun, Y. S. Chai, Y. S. Oh, D. Jaiswal-Nagar, S. Y. Haam, I. Kim, B. Lee, D. H. Nam, K.-T. Ko, J.-H. Park, *Physical review letters* **104**, 037204 (2010).
- [39] Q. He, T. Yuan, X. Zhang, X. Yan, J. Guo, D. Ding, M. A. Khan, D. P. Young, A. Khasanov, Z. Luo, *The Journal of Physical Chemistry C* **118**, 24784 (2014).
- [40] C. Wang, X. Han, P. Xu, J. Wang, Y. Du, X. Wang, W. Qin, T. Zhang, *The Journal of Physical Chemistry C* **114**, 3196 (2010).
- [41] X. Li, R. Gong, Z. Feng, J. Yan, X. Shen, H. He, *Journal of the American Ceramic Society* **89**, 1450 (2006).
- [42] Z. Haijun, Y. Xi, Z. Liangying, *Journal of the European Ceramic Society* **22**, 835 (2002).
- [43] M. Chua, Z. Yang, Z. Li, *Journal of Magnetism and Magnetic Materials* **368**, 19 (2014).
- [44] A. Yusoff, M. Abdullah, S. Ahmad, S. Jusoh, A. Mansor, S. Hamid, *Journal of Applied Physics* **92**, 876 (2002).

*Corresponding author: a.s.h.rozatian@phys.ui.ac.ir.